Journal Name

ARTICLE TYPE

Cite this: DOI: 00.0000/xxxxxxxxxx

Supporting Information - Gold Doping of Tin Clusters: Exo- vs Endohedral Complexes†

Martin Gleditzsch,*[a] Lukáš F. Pašteka,[b], Daniel A. Götz[a], Armin Shayeghi[c], Roy L. Johnston[d] and Rolf Schäfer[a]

Received Date
Accepted Date

DOI: 00.0000/xxxxxxxxxx

We present molecular beam electric deflection experiments on neutral gold-doped tin clusters. The experimental Sn_NAu ($N = 6-16$) cluster beam profiles are interpreted by means of classical trajectory simulations supplied, with cluster structures generated by a genetic algorithm based on density functional theory. The combined experimental and theoretical analysis confirms that at least nine tin atoms are necessary to form a cage that is capable of encapsulating a gold atom, with high symmetry only marginally distorted by the gold atom. Two-component DFT calculations reveal that spin-orbit effects are necessary to properly describe these species. Partial charge analysis methods predict the presence of charge transfer effects.

1 Electric Beam Deflection

An exemplary mass spectrum of gold-doped tin clusters for an alloy target (15 atom-% Au in Sn) at 20 K nozzle temperature is shown in Figure 1. The mass signals for $N = 6-9$ are relatively small and difficult to stabilize during the beam deflection measurement. Starting with $N = 10$, the doped species display heightened intensities and are more stable during the deflection measurements. The species $N = 10, 12$ display the highest signal intensity. This is also reflected in the relative stabilities of the predicted ground states, as seen in Figure 5. Larger as well as double-doped species are also abundant, but cannot be measured due to the low intensity in the beam and the broad isotopic distribution of tin. Figure 2 illustrates the influence of the rotational temperature on two electric beam deflection simulations. The influence is shown to be only minor in the range $T_{\mathrm{rot}} = 5-25$ K. Thus, the assumption $T_{\mathrm{rot}} = 10$ K is appropriate and employed for all simulations shown in the main text.

2 Quantum Chemistry

Figure 3 and 4 show all energetically low-lying isomers up to 0.5 eV for Sn_NAu with $N = 6-16$. All structures have been obtained by optimizing the GA generated candidates with density functional theory (DFT) on the PBE0/cc-pVTZ-PP level of theory. All low lying structures were found to possess doublet multiplicity, as their corresponding quartet structures were at least 0.7 eV higher in energy. Their properties are summarized in table 1. The first column contains the label as shown in Figure 3 and 4. ΔE refers to the energy relative with respect to the identified global minimum structure in eV, which is followed by the column for the point group symmetry (Symm.). The columns for the total magnitude of the electric dipole moment μ_{tot} and its components μ_i ($i = x, y, z$) are displayed in Debye (D) and in the same molecular fixed frame like the moment of inertia components I_i ($i = x, y, z$) (which are expressed with respect to the smallest component I_{min} in kg m$^2 \cdot 10^{-44}$). The average binding energy E_b has been calculated by equation 1 and is shown together with the second order energy difference $\Delta^2 E$ from equation 2 as well as μ_{tot} in Figure 5. Starting with ten tin atoms, the average binding energy seems to approach a near constant value. This suggests that starting with ten tin atoms the gold-doped species display a heightened stability, which is reflected in the stability of the clusters during the electric deflection measurement. The second order energy differences further reveal, that $Sn_{10}Au$ and $Sn_{12}Au$ are especially stable from a quantum chemical perspective. This agrees well with the mass peak intensities, as the corresponding peaks display the highest signals of all doped clusters.

$$E_b = (E(Sn_{(N)}Au) - N \cdot E(Sn) - E(Au))/(N+1) \quad (1)$$

$$\Delta^2 E = 2 \cdot E(Sn_{(N)}Au) - E(Sn_{(N+1)}Au) - E(Sn_{(N-1)}Au) \quad (2)$$

[a] Technische Universität Darmstadt, Eduard-Zintl-Institut, Alarich-Weiss-Straße 8, 64287 Darmstadt, Germany
[b] Department of Physical and Theoretical Chemistry & Laboratory for Advanced Materials, Faculty of Natural Sciences, Comenius University, Mlynská dolina, Ilkovičova 6, 84215 Bratislava, Slovakia
[c] Vienna Center for Quantum Science and Technology (VCQ), Faculty of Physics, University of Vienna, Boltzmanngasse 5, A-1090 Vienna, Austria
[d] School of Chemistry, University of Birmingham, Edgbaston, Birmingham B15 2TT, United Kingdom

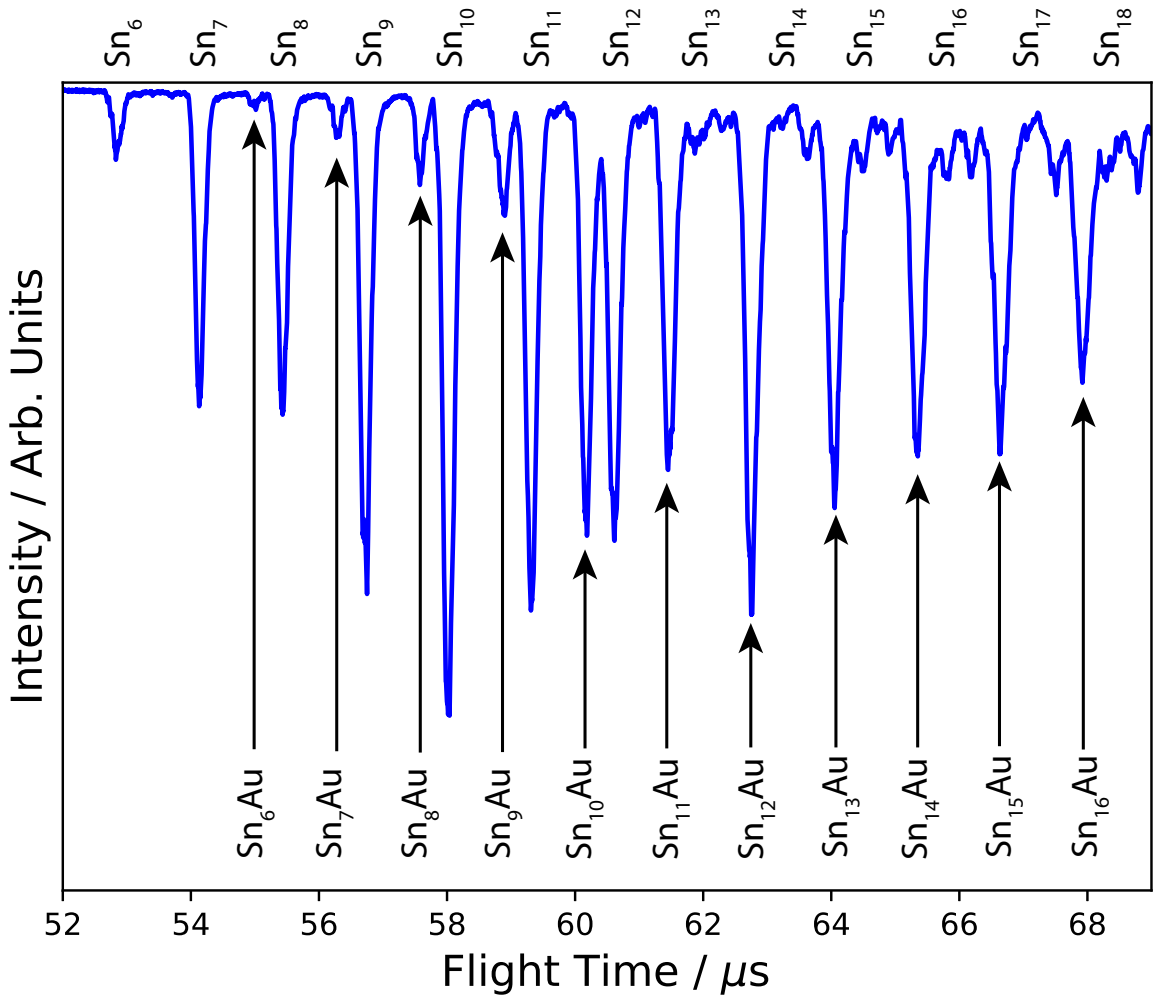

Fig. 1 Mass spectrum of gold-doped tin clusters Sn_NAu for an alloy target (15 atom-% Au in Sn) at 20 K nozzle temperature. The mass signals for pure tin clusters are shown as reference. While the smaller doped species with $N > 10$ display low intensities and are difficult to stabilize in deflection measurements, starting with $N = 10$, the doped species display heightened intensities and stability during the deflection measurements. The mass signals corresponding to $N = 10, 12$ display the highest signal intensity of the doped species.

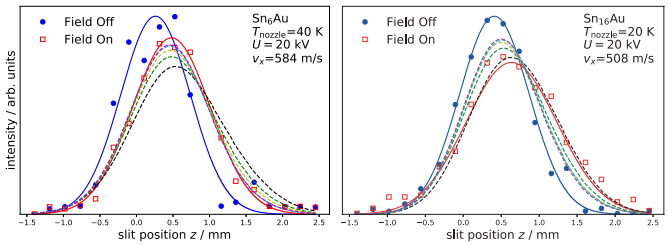

Fig. 2 Comparison of experimental electric deflection results with field switched off (blue) and on (red) with the simulated beam profiles for different rotational temperatures (T_{rot}). The influence on a rigid rotor is shown to be only minor in the range of 5-25 K. The colour notation is black (5 K), green (10 K), yellow (15 K), cyan (20 K) and magenta (25 K).

Table 1 Results of the DFT studies for Sn_NAu on the PBE0/cc-pVTZ-PP level of theory. All structures have doublet spin multiplicity.

Label	ΔE/eV	Symm.	μ_{tot} /D	μ_x/D	μ_y/D	μ_z/D	$\frac{I_{min}}{(kg\cdot m^2\cdot 10^{-44})}$	I_x/I_{min}	I_y/I_{min}	I_z/I_{min}
6-I	0.00	C_s	0.30	0.00	0.29	0.05	4.663	1.000	1.095	1.357
6-II	0.09	C_s	0.09	−0.07	−0.06	0.00	4.040	1.000	1.446	1.402
6-III	0.11	C_s	0.58	0.58	0.00	0.00	4.430	1.000	1.012	1.496
6-IV	0.33	C_1	0.20	0.05	−0.10	−0.17	3.489	1.000	1.880	2.192
6-V	0.42	C_s	1.19	−1.17	0.00	−0.16	4.118	1.000	1.395	1.545
7-I	0.00	C_s	0.39	0.38	0.00	0.09	5.019	1.000	1.480	1.832
7-II	0.27	C_1	0.31	−0.10	0.04	0.28	5.099	1.000	1.640	1.365
7-III	0.31	C_s	0.80	0.58	0.00	0.55	5.362	1.000	1.198	1.528
8-I	0.00	C_s	0.08	0.00	0.04	−0.07	6.022	1.000	1.448	1.643
8-II	0.01	C_s	0.32	−0.10	0.00	−0.30	6.891	1.000	1.300	1.353
8-III	0.04	C_1	0.24	0.00	−0.22	−0.09	5.866	1.000	2.152	1.841
8-IV	0.19	C_s	0.29	−0.29	0.01	0.00	6.802	1.000	1.468	1.355
8-V	0.22	C_2	0.43	0.00	0.00	−0.43	5.801	1.000	1.904	1.667
8-VI	0.22	C_s	0.36	0.06	0.00	0.35	6.621	1.000	1.162	1.538
8-VII	0.34	C_1	0.53	0.33	0.39	−0.15	6.777	1.000	1.207	1.391
9-I	0.00	C_s	0.41	0.00	0.40	0.10	8.364	1.000	1.034	1.296
9-II	0.39	C_s	0.31	0.00	−0.01	0.31	8.906	1.000	1.069	1.287
9-III	0.46	C_1	0.25	0.10	−0.22	−0.05	9.277	1.000	1.039	1.260
10-I	0.00	D_{4d}	0.00	0.00	0.00	0.00	9.973	1.000	1.076	1.076
11-I	0.00	C_s	0.24	0.00	0.11	0.21	11.691	1.000	1.072	1.137
11-II	0.27	C_s	0.66	0.64	−0.17	0.00	10.625	1.000	1.277	1.423
11-III	0.41	C_{2v}	0.09	0.09	0.00	0.00	11.293	1.000	1.133	1.343
12-I	0.00	D_{5d}	0.00	0.00	0.00	0.00	14.023	1.000	1.000	1.029
13-I	0.00	C_s	0.93	0.89	0.00	−0.27	14.483	1.000	1.244	1.256
13-II	0.24	C_1	0.91	0.85	0.24	−0.21	13.164	1.000	1.456	1.602
13-III	0.49	C_s	1.36	−1.28	0.00	−0.45	13.432	1.000	1.434	1.515
13-IV	0.41	C_s	0.45	0.00	−0.02	0.45	12.898	1.000	1.520	1.708
14-I	0.00	C_s	0.63	0.44	0.00	0.45	15.370	1.000	1.371	1.457
14-II	0.16	C_s	0.64	−0.63	0.00	−0.08	14.834	1.000	1.536	1.644
14-III	0.24	C_2	0.08	0.00	0.08	0.00	16.159	1.000	1.302	1.423
14-IV	0.28	C_1	0.73	0.70	−0.11	−0.18	15.469	1.000	1.397	1.491
14-V	0.32	C_s	1.22	1.21	0.09	0.00	17.309	1.000	1.094	1.336
14-VI	0.48	C_1	0.62	−0.49	0.38	−0.04	16.830	1.000	1.144	1.400
15-I	0.00	C_s	0.56	0.34	0.44	0.00	17.631	1.000	1.384	1.397
15-II	0.20	C_s	0.45	0.27	0.36	0.00	16.810	1.000	1.570	1.595
15-III	0.22	C_1	1.04	−0.69	0.75	0.21	17.641	1.000	1.328	1.434
15-IV	0.24	C_s	1.15	1.14	0.00	−0.10	15.576	1.000	1.795	1.819
15-V	0.28	C_1	1.59	1.48	−0.53	−0.28	19.012	1.000	1.161	1.365
15-VI	0.34	C_{2v}	0.24	−0.24	0.00	0.00	20.428	1.000	1.006	1.157
15-VII	0.37	C_1	0.77	0.30	0.71	−0.01	18.527	1.000	1.239	1.363
15-VIII	0.38	C_{2v}	0.57	0.00	0.57	0.00	18.857	1.000	1.141	1.335
15-IX	0.46	C_s	0.61	−0.53	0.00	0.30	18.721	1.000	1.215	1.384
16-I	0.00	C_s	0.38	0.05	0.00	−0.38	18.214	1.000	1.584	1.637
16-II	0.05	C_s	0.45	0.00	−0.09	0.44	20.354	1.000	1.275	1.483
16-III	0.11	C_s	0.65	0.49	−0.42	0.00	23.458	1.000	1.083	1.105
16-IV	0.12	C_1	0.68	0.61	−0.10	0.29	21.638	1.000	1.154	1.346
16-V	0.15	C_2	0.34	−0.34	0.00	0.00	21.262	1.000	1.130	1.335
16-VI	0.16	C_s	1.47	1.38	−0.49	0.00	18.058	1.000	1.744	1.749
16-VII	0.25	C_s	1.08	1.05	0.00	−0.25	18.066	1.000	1.745	1.762

Furthermore, we present the results of different partial charge analysis methods in table 1. Here δ_i are the partial charges and ρ_i the total spin density on the gold dopant. The employed methods are the 'density derived electrostatic and chemical approach' (DDEC6), Löwdin population analysis (Löw.), natural bond order analysis (NBO) and Bader charge (Bad.) analysis. Both the techniques based on partitioning of the electron density distribution and methods based on wave function analysis reveal negative partial charges on the gold dopant. Thus, the gold dopant is inducing a negative charge transfer which is more pronounced for endohedral structures. Only the amount of the transferred charge can not be verified. Additionally, the total spin density displays consistent values for all applied techniques and with the exception of Sn_9Au all endohedral structures display a vanishing spin density at the gold dopant. This makes the spin density a further indication for the observed change in the structural motif.

Table 2 Results of the ground state partial charge analysis for Sn_NAu on the PBE0/cc-pVTZ-PP level of theory. Here δ_i are the partial charges (or net atomic charges, NAC) and ρ_i the total spin density on the gold dopant for 'density derived Electrostatic and chemical approach' (DDEC6), Löwdin (Löw), Natural Charge (Nat) and Bader analysis, respectively. The endohedral structures ($N > 8$) show increased partial charges at the location of the dopant as well as a vanishing spin density (with the exception of Sn_9Au).

N	δ_{DDEC6}	ρ_{DDEC6}	$\delta_{Löw}$	$\rho_{Löw}$	δ_{NBO}	ρ_{NBO}	$\delta_{Bad.}$
6	−0.02	0.04	−0.23	−0.03	−0.20	−0.03	−0.52
7	−0.05	0.22	−0.29	0.08	−0.15	0.18	−0.49
8	−0.15	0.04	−0.32	0.09	−0.77	0.03	−0.75
9	−0.33	0.09	−0.61	0.11	−2.13	0.10	−1.13
10	−0.29	0.01	−0.73	0.04	−3.16	−0.04	−1.45
11	−0.30	0.00	−0.69	0.02	−2.75	−0.04	−1.20
12	−0.28	−0.01	−0.69	0.01	−2.75	−0.04	−1.14
13	−0.25	−0.01	−0.70	0.00	−2.65	0.00	−1.13
14	−0.27	−0.01	−0.67	0.00	−2.44	−0.01	−1.11
15	−0.25	−0.01	−0.64	0.01	−2.34	0.00	−1.09
16	−0.25	−0.02	−0.67	−0.01	−2.36	0.00	−1.07

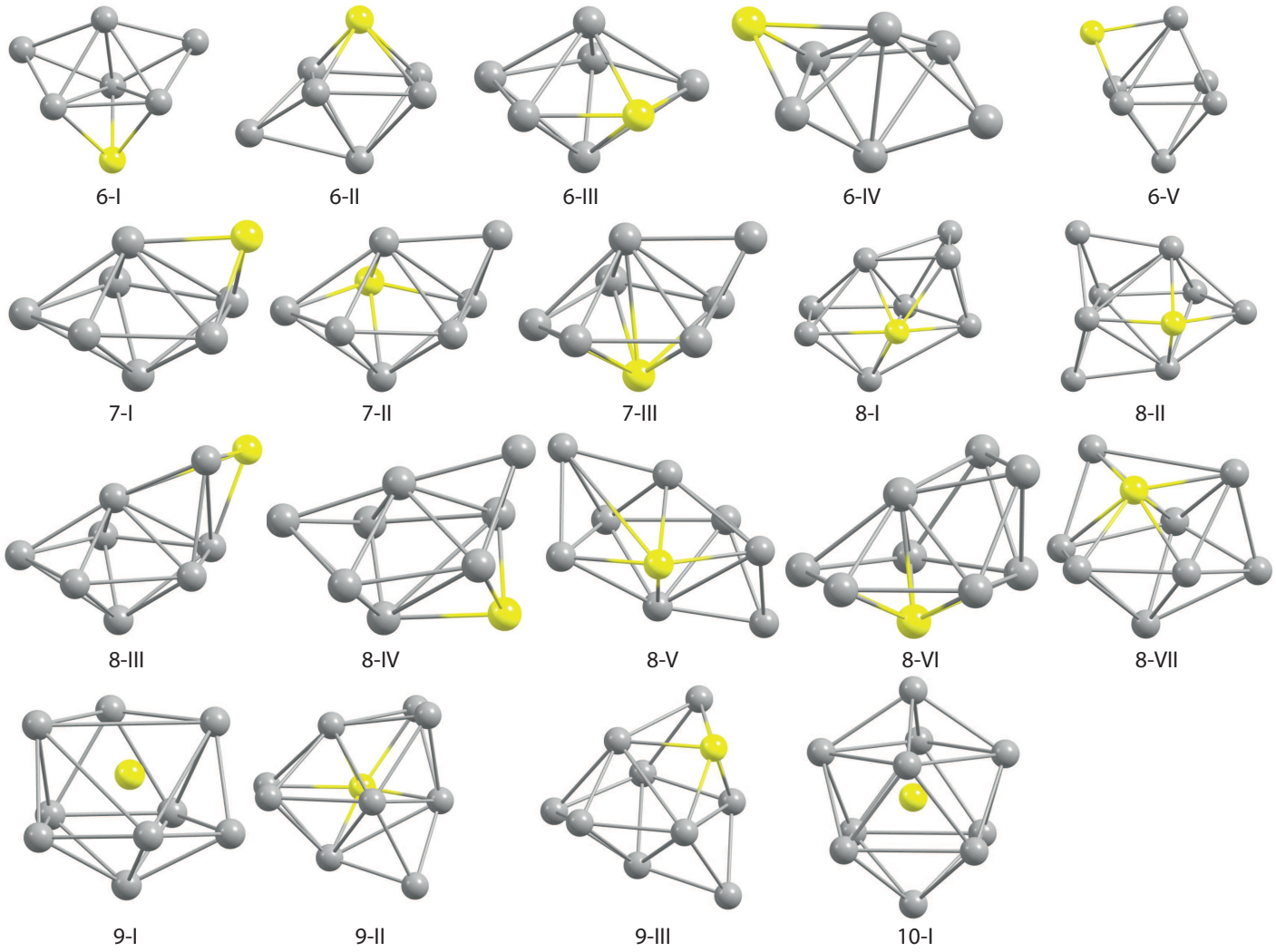

Fig. 3 Energetically low-lying isomers up to 0.5 eV for the single-doped Sn_NAu clusters with $N = 6 - 10$ as obtained at the PBE0/cc-pVTZ-PP level of theory with DFT. Below each structure, the number of tin atoms and the order of the isomer (roman numeral) is denoted. Their corresponding properties are summarized in table 1.

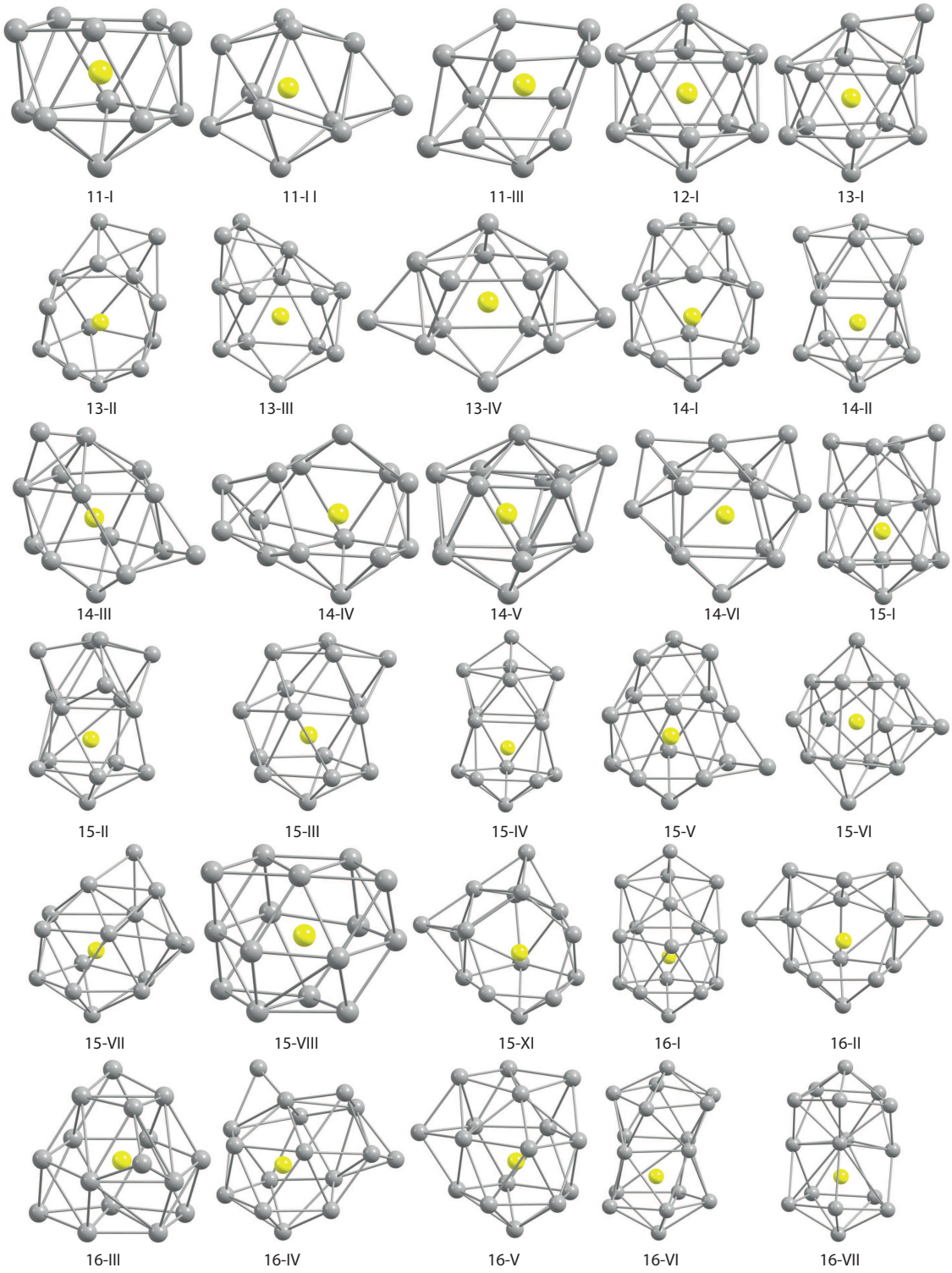

Fig. 4 Energetically low-lying isomers up to 0.5 eV for the single-doped Sn_NAu clusters with $N = 11 - 16$ as obtained at the PBE0/cc-pVTZ-PP level of theory with DFT. The notation is equivalent to Figure 4 Their corresponding properties are summarized in table 1.

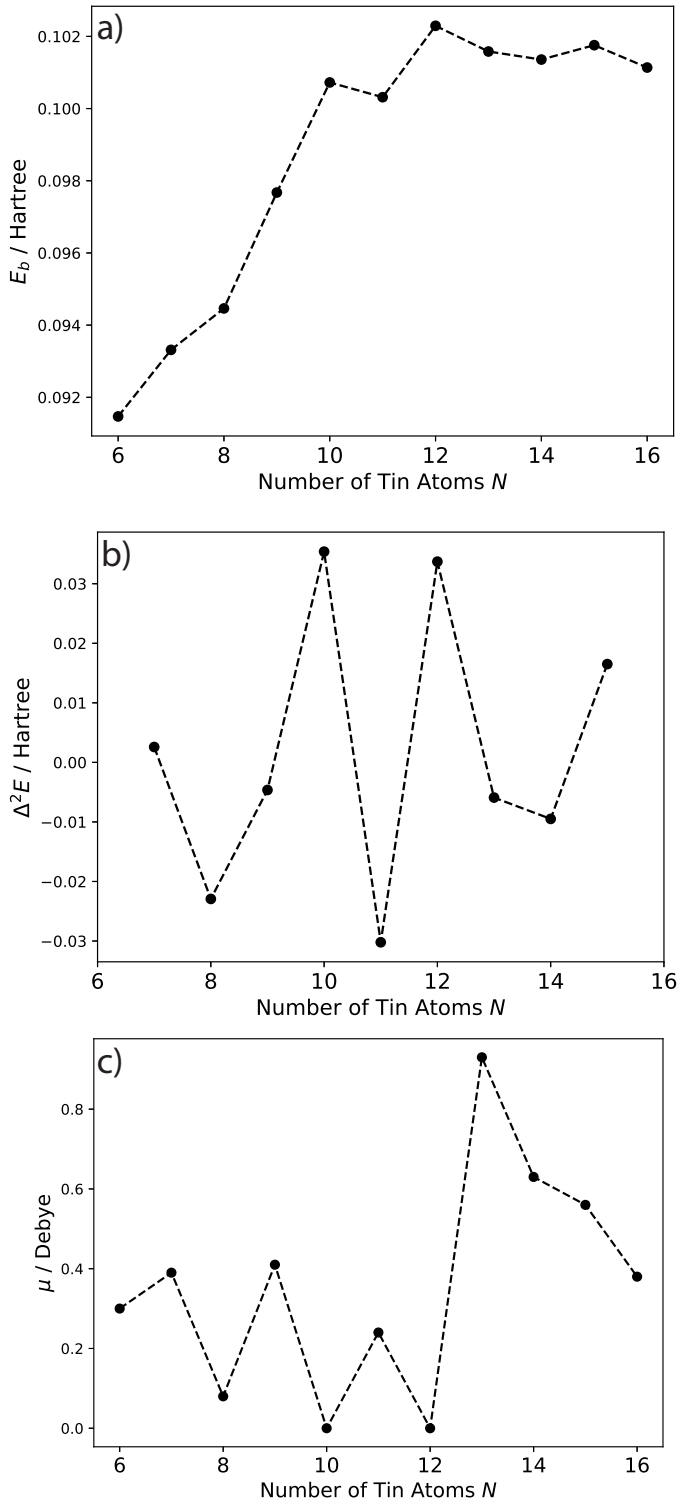

Fig. 5 Subfigure (a) shows the average binding energy E_b as a function of the number of tin atoms N. Starting with ten tin atoms, E_b approaches a constant value. The second order energy difference $\Delta^2 E$ in Subfigure (b) reveals that the species with ten and twelve tin atoms are especially stable. The dipole moment μ in Subfigure (c) is insensitive to the structural transition from exohedral ($N = 8$) to endohedral complexes ($N = 9$). The species with ten and twelve tin atoms display vanishing dipole moments. The calculations have been done for the identified DFT ground states on the PBE0/cc-pVTZ-PP level of theory.